crystals

MDPI

Article

A 0D/2D Heterojunction Composite of Polymeric Carbon Nitride and ZIF-8-Derived ZnO for Photocatalytic Organic Pollutant Degradation

Vandana P. Viswanathan [1], Vaishak T. Balakrishnan [1], Nayarassery N. Adarsh [1,2,*], Binsy Varghese V [3] and Suresh Mathew [1,4,*]

[1] School of Chemical Sciences, Mahatma Gandhi University, Kottayam 686560, India
[2] Chemistry and Biomolecular Science, Clarkson University, 8 Clarkson Ave., Potsdam, NY 13699, USA
[3] St. Joseph's College, Irinjalakuda 680125, India
[4] Advanced Molecular Materials Research Centre (AMMRC), Mahatma Gandhi University, Kottayam 686560, India
* Correspondence: adarshnn@gmail.com (N.N.A.); smathew1962@gmail.com (S.M.)

Abstract: Solar photocatalytic technology based on semiconducting materials has gained the attention of the scientific community to solve the energy crisis and environmental remediation. Zeolitic imidazolate frameworks (ZIFs) are a subfamily of metal–organic frameworks (MOFs) with the isomorphic topologies of zeolites and coordinative compositions of MOFs. Owing to high specific surface areas, tunable channels and high thermal stabilities, zeolitic imidazolate frameworks (ZIFs) have been used in catalytic applications. In this paper, ZIF-8 was used as a matrix to synthesize 0D/2D heterojunction photocatalysts, viz., ZnO/C_3N_4-x% (x = 2.5, 5 and 10), for the photocatalytic degradation study of rhodamine B (RhB). The synthesized composite materials were characterized using FTIR, PXRD, UVDRS, PL, TEM, and BET analyses. TEM images showed the nearby contacts between ZnO and C_3N_4 in the hybrid and the uniform distribution of ZnO on the surface of the C_3N_4 nanosheet, thus increasing the development of 0D/2D heterojunction. The hybrid system ZnO/C_3N_4-5% (ZCN-5) showed good photocatalytic activity for the degradation of RhB under sunlight. A possible mechanism for the improved photocatalytic activity of the ZnO/C_3N_4 composite is also suggested. This exploratory study demonstrates the effective separation and migration of photo-induced electron–hole pairs between the 2D C_3N_4 sheet and 0D ZnO for the improved performance of heterojunction photocatalysts.

Keywords: heterojunction; ZIF-8; ZnO; polymeric carbon nitride; photocatalyst

check for updates

Citation: Viswanathan, V.P.; Balakrishnan, V.T.; Adarsh, N.N.; Varghese V, B.; Mathew, S. A 0D/2D Heterojunction Composite of Polymeric Carbon Nitride and ZIF-8-Derived ZnO for Photocatalytic Organic Pollutant Degradation. *Crystals* **2023**, *13*, 47. https://doi.org/10.3390/cryst13010047

Academic Editor: Dah-Shyang Tsai

Received: 17 November 2022
Revised: 16 December 2022
Accepted: 21 December 2022
Published: 27 December 2022

Copyright: © 2022 by the authors. Licensee MDPI, Basel, Switzerland. This article is an open access article distributed under the terms and conditions of the Creative Commons Attribution (CC BY) license (https://creativecommons.org/licenses/by/4.0/).

1. Introduction

Heterogeneous semiconductor photocatalysis has emerged as one of the utmost effective green technologies for the removal of organic pollutants [1]. In this context, several researchers are working on the advance of nanostructured metal oxides having improved photocatalytic properties [2]. Concerning various metal oxides, zinc oxide (ZnO) raised interest among many material chemists owing to its wide bandgap of 3.37 eV, biocompatibility, high absorption of ultraviolet radiation at ambient temperature, large exciting binding energy (60 meV) [3], and its promising applications such as in sensors [4], piezoelectric devices [5], solar cells [6], antimicrobial agents [7], photocatalysts [8], and photodetectors [9]. More interestingly, ZnO also serves as a photocatalyst for the degradation of organic pollutants because of its environmental friendliness, low cost, and high activity [10–12]. Nevertheless, ZnO has shown two limitations in photocatalytic activity owing to its large bandgap and a fast rate of charge-carrier recombination of photogenerated electrons–hole pairs with low quantum efficiency. Thus, to overcome these issues, and to further expand the absorption spectrum to the visible region for the photocatalytic degradation of

organic pollutants, various methods were explored by research groups for synthesizing novel Z-scheme photocatalysts [13–15], doping ZnO with other metallic or non-metallic elements [16–18], and coupling with other semiconductors [19].

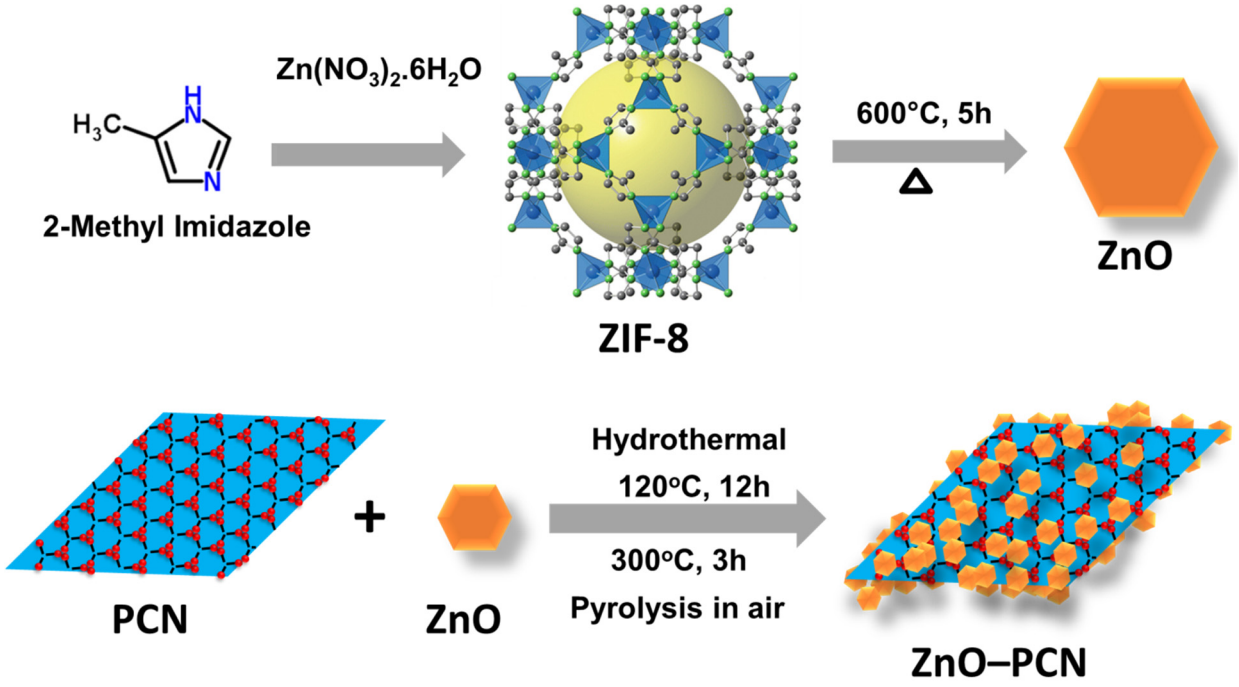
Polymeric carbon nitride (C_3N_4) has attracted attention as a potential metal-free photocatalytic material due to having a suitable bandgap (2.7 eV) for visible light absorption [20–24] and exhibited potential photocatalytic applications in organic pollutant degradation [25], chemical sensing [26], water splitting [27–29], and photovoltaic solar cell [30]. Despite these interesting characteristics, C_3N_4 is facing a few drawbacks such as less surface-to-volume ratio, poor quantum yield, and fast photogenerated charge carrier recombination rate. A heterojunction composite built from the combination of ZnO and C_3N_4 is one of the excellent strategies for the construction of a viable semiconductor-based photocatalyst [31]. Such a nanocomposite can solve the individual drawbacks of ZnO and C_3N_4 and acts as a potential photocatalyst for the effective degradation of rhodamine B (RhB). Based on the dimensionality of the nanostructures of ZnO and C_3N_4, various research groups presented their results in the literature on 0D/2D [32–36], 1D/0D [37], 1D/2D [38–43], 2D/0D [44], 2D/2D [45], and 3D/2D [31] heterojunction composites (where 0D, 1D, 2D, and 3D are zero-, one-, two-, and three-dimensional composites) involving ZnO and C_3N_4, respectively. Sharma et al. designed a ZnO/g-C_3N_4 photocatalyst for the removal of methylene blue (MB). The ZnO/g-C_3N_4 composite degraded MB by 90% for 120 min under visible light [46]. A novel photocatalyst using ZnO/sulfur-doped C_3N_4 was also reported for the degradation of MB under sunlight. The degradation efficiency of the composite was shown as 93% for 80 min [47]. Zhu et al. studied the photocatalytic degradation of tetracycline hydrochloride using ZnO/g-C_3N_4, which degraded 97% for 30 min under UV light [39]. Moussa and coworkers developed a ZnO/g-C_3N_4 photocatalyst for the removal of orange II. The degradation efficiency reached 100% for 300 min [48]. Zirong and coworkers revealed the photocatalytic efficiency of ZnO derived from metal–organic framework ZIF-8 with C_3N_4 for the removal of methyl orange. They found that the degradation efficiency of the composite reached 100% for 20 min under UV light [49].

We are interested in 0D/2D heterojunction composites of ZnO/C_3N_4 due to the following reasons: (1) The 0D nanoparticles of ZnO can be dispersed and bind over the surface of 2D porous nanosheet of C_3N_4; (2) the interfacial contact between the heterojunction of 0D ZnO and 2D C_3N_4 are very strong and are responsible for the separation of photogenerated charge carriers; (3) the 0D ZnO nanoparticles can afford additional active sites on the nanosheet surface of 2D C_3N_4. This helps to decrease the distance of diffusion of photogenerated charges; (4) the porous structure of ZnO/C_3N_4 nanoheterojunction will enhance the catalyst to adsorb the organic pollutant and further promote degradation; (5) both ZnO and C_3N_4 are environmentally friendly and cost-effective nanomaterials and will help the development of sustainable photocatalysts; and (6) 0D/2D heterojunction composites of ZnO/C_3N_4 have been used for several intriguing applications such as water decontamination [20a], organic pollutant degradation, photocatalytic hydrogen evolution and photocatalytic decomposition of N_2O [50].

Metal–organic frameworks (MOFs) [51–53] or porous coordination polymers (PCPs) [54–56] are intriguing crystalline materials due to their remarkable specific surface area, high chemical and thermal stability, robust framework structure, and tunable porosities. MOFs have been considered successful candidates as sacrificial templates for the synthesis of carbonaceous metal oxides and have been used in various applications such as electrode materials for supercapacitors [57–59], batteries [60–62], photocatalysts [63,64], sensors [65,66], and for gas adsorption [67,68], due to their high surface area and well-defined pore shape/size. In contrast to other methods, metal oxides synthesized by using MOFs as the precursor template showed more advantages such as high surface area and uniform porous structure, which offers many active reaction sites, short charge diffusion sites, and more consistency during electrochemical or photochemical reactions. Dong and coworkers reported a ZnO/C_3N_4 heterojunction composite for the first time by using ZIF-8 (zeolitic imidazolate framework-8, one of the subfamilies of MOFs) [69,70] as the precursor

material. Interestingly, a ZnO/C_3N_4 composite showed promising anode material for sodium-ion batteries [71]. Recently, Aleksandrzak et al. assembled a ZnO/C_3N_4 composite by mixing carbonized ZnO derived from MOF-5 [72] (via thermolysis at 700 °C) with bulk C_3N_4, which showed excellent photocatalytic hydrogen evolution performance [73].

In the present study, we synthesized a 0D/2D heterojunction photocatalyst, ZnO/C_3N_4-x% (x = 2.5, 5, and 10), encompassing ZnO derived from ZIF-8 and C_3N_4 sheets (Scheme 1). The synthesized material showed better performance as a heterojunction photocatalyst owing to the interfacial coupling between the 2D C_3N_4 sheet and 0D ZnO, which reduced the separation of charge carriers. In our work, ZnO derived from ZIF-8 with C_3N_4 showed excellent performance for the degradation of rhodamine B. The degradation rate of RhB reached 95% within 70 min under sunlight compared with other reported work (Table S1).



Scheme 1. Schematic representation of the synthesis of the composites of ZnO/C_3N_4.

2. Experimental Section

2.1. Materials

Urea (99%, Merck Specialties Pvt. Ltd., Mumbai, India, $Zn(NO_3)_2 \cdot 6H_2O$ (99%, Sigma Aldrich, Burlington, MA, USA), 2-methylimidazole (99%, Sigma Aldrich), hydrogen peroxide (30%, Merck Specialties Pvt. Ltd.), and methanol (99.8%, Sigma Aldrich) were used.

2.2. Synthesis of ZnO Derived from ZIF-8

Briefly, 20 mmol 2-methylimidazole and 5 mmol $Zn(NO_3)_2 \cdot 6H_2O$ were separately dissolved in 50 mL methanol for 15 min using a sonicator. The $Zn(NO_3)_2 \cdot 6H_2O$ solution was poured into the 2-methylimidazole solution, and the resulting mixture was allowed to gel under stirring. The solution was stirred for 3 h and then kept standing at room temperature for 24 h. The crystallized ZIF-8 was centrifuged and washed with 15 mL of methanol. The synthesized ZIF-8 was heated at 600 °C for 5 h at a heating rate of 2 °C min^{-1}, yielding ZnO.

2.3. Synthesis of Polymeric Carbon Nitride (C_3N_4)

Briefly, 10 g urea was placed in a crucible with a cover and pyrolyzed at 530 °C for 4 h in air at a ramp rate of 3 °C min^{-1}, resulting in the yellow polymeric carbon nitride.

2.4. Synthesis of ZnO/C_3N_4

For synthesis, 100 mg of ZIF-8-derived ZnO was added into a 10 mL methanol solution, forming solution A, and C_3N_4 was dissolved in 10 mL methanol, forming solution B. Then, solution A was added dropwise into solution B, and the suspension was stirred for 30 min. The resulting solution was heated to 120 °C for 12 h under hydrothermal conditions. The ZnO/C_3N_4-x% (x = 2.5, 5, and 10) was again heated at 300 °C for 4 h in a muffle furnace in air. The as-prepared ZnO/C_3N_4 composite with 5% of C_3N_4 was denoted as ZCN-5. For comparison, composites with 2.5% and 10% of C_3N_4 were also produced and designated as ZCN-2.5 and ZCN-10, respectively.

2.5. Characterization

Fourier transform infrared (FTIR) spectroscopy was used for analysis using a Perkin Elmer 400 Spectrometer. The crystalline phase was characterized via X-ray diffraction using a Rigaku Miniflex 600 powder X-ray diffractometer with monochromatized Cu Kα (λ = 1.5425 Å) incident radiation. The UV–Vis diffuse reflectance spectra (UVDRS) of the composites were scanned using a UV 2450 Shimadzu UV–Vis spectrophotometer. Photoluminescence spectra (PL) of the samples were obtained using a fluorescence spectrometer (Shimadzu RF-5301 spectrofluorometer) at room temperature excited at a wavelength of 320 nm. SEM images were obtained using a JEOL JEM-2100 microscope (Tokyo, Japan) at an accelerating voltage of 200 kV. The morphology and fine structure of materials were employed through transmission electron microscopy (JEOL-1400 operated at 120 kV). The Brunauer–Emmet–Teller (BET, Nova Touch Lx2 by quantachrome) was used to calculate the specific area, pore size, and pore volume. X-ray photoelectron spectroscopy was performed with an X-ray photoelectron spectrometer (XPS, NEXSA surface analysis, Source Al Monochromatic energy 1486.6 eV).

3. Results and Discussion

The FTIR spectra of ZnO, C_3N_4, and its composites, namely ZCN-2.5, ZCN-5, and ZCN-10 hybrids, are provided in Figure 1. Two peaks at 513 cm^{-1} and 431 cm^{-1} corresponding to the stretching vibrations of Zn-O were observed. The spectrum of C_3N_4 exhibited absorption peaks at 3176 and 809 cm^{-1}, which were assigned to the stretching vibrations of N-H and s-triazine unit modes. The stretching vibration bands of C-N/C=N and tensile vibration modes of C-N heterocyclic rings were observed in the spectrum ranging from 1756 to 1113 cm^{-1}. There were characteristic peaks of both ZnO and C_3N_4 observed in the FTIR spectra of the ZnO/C_3N_4 composite photocatalyst. The absorption peaks at 1236, 1317, 1406, 1459, and 1640 cm^{-1} were correlated with the stretching vibration of aromatic C=N as well as the breathing mode of the C-N heterocycles of C_3N_4 [74,75].

As shown in Figure 2, ZnO showed various diffraction peaks at 31.7°, 34.3°, 36.3°, 47.8°, 56.6°, 62.7°, 68.3°, and 69.3°, corresponding to (100), (002), (101), (102), (110), (103), (200), and (112) lattice planes of ZnO (JCPDS file: 36-1451), indicating that the ZIF-8 was oxidized to ZnO with high purity during the calcination process. The peaks at 12.9° and 27.6° in the XRD patterns, corresponding to (100) and (002) lattice planes, confirmed the presence of C_3N_4. (JCPDSF No. 87-1526). No diffraction peaks of C_3N_4 were observed in ZnO/C_3N_4 composites because of the small amount of C_3N_4 [33,76].

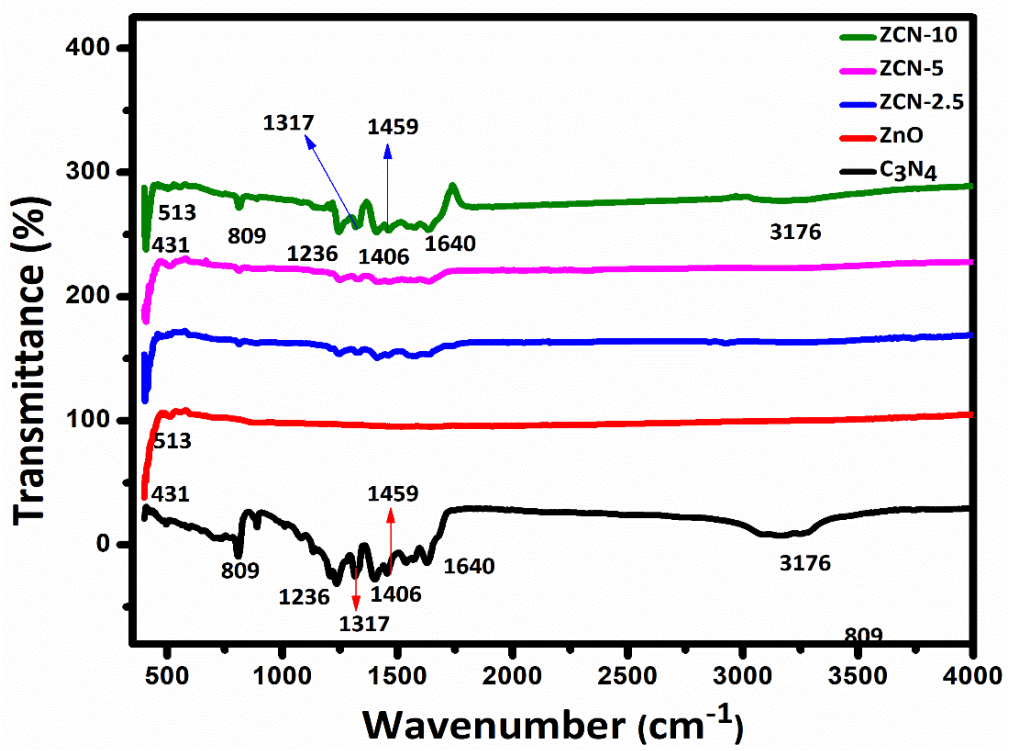


Figure 1. The FTIR spectra of ZnO, C_3N_4, and composites of ZnO/C_3N_4.

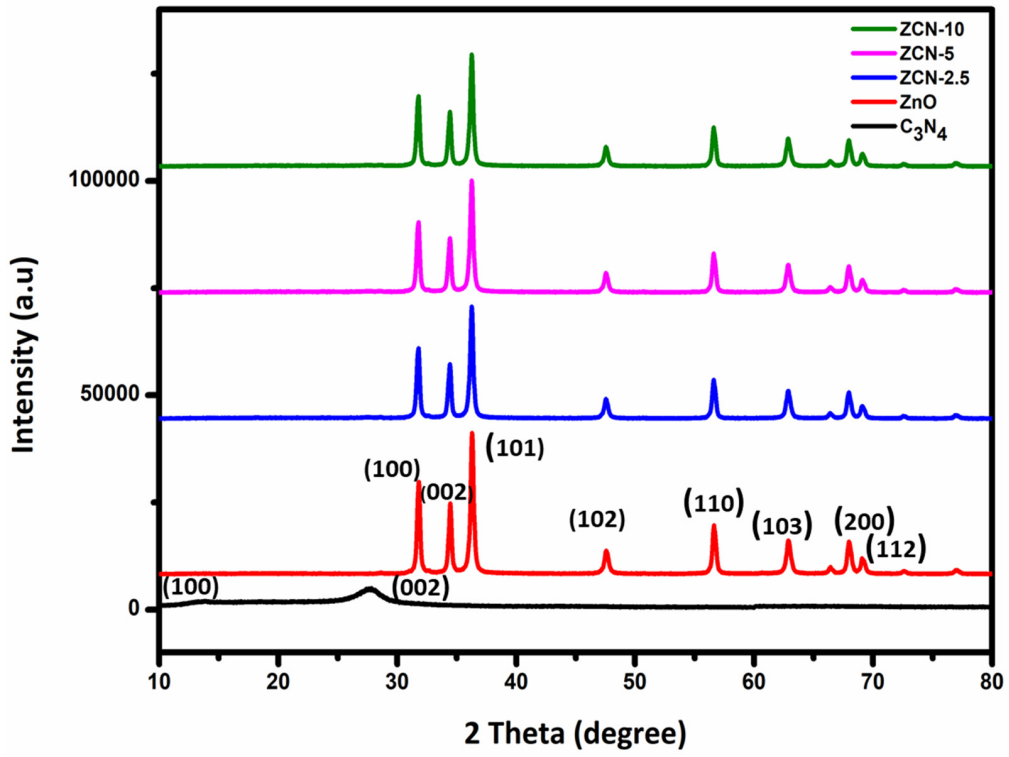


Figure 2. The PXRD patterns of ZnO and composites of ZnO/C_3N_4.

The optical properties of ZnO, C_3N_4, and ZnO/C_3N_4 photocatalysts were studied using UV–Vis diffuse reflectance spectra, as shown in Figure 3a. The absorption edge of ZnO and ZnO/C_3N_4 composites (ZCN-5) were observed at 399 nm and 450 nm, respectively. The absorption edge of the ZnO/C_3N_4 hybrid (ZCN-5) shifted to a longer wavelength of 450 nm compared with ZnO. The bandgap energy of these materials was determined

using the Tauc plot (Figure 3b), and it was estimated to be 3.25 eV and 2.91 eV for ZnO and ZCN-5, respectively. The lowering of the bandgap to 2.91 eV for ZnO/C_3N_4 composites (ZCN-5) is due to the strong interfacial coupling between ZnO and C_3N_4 [77,78].

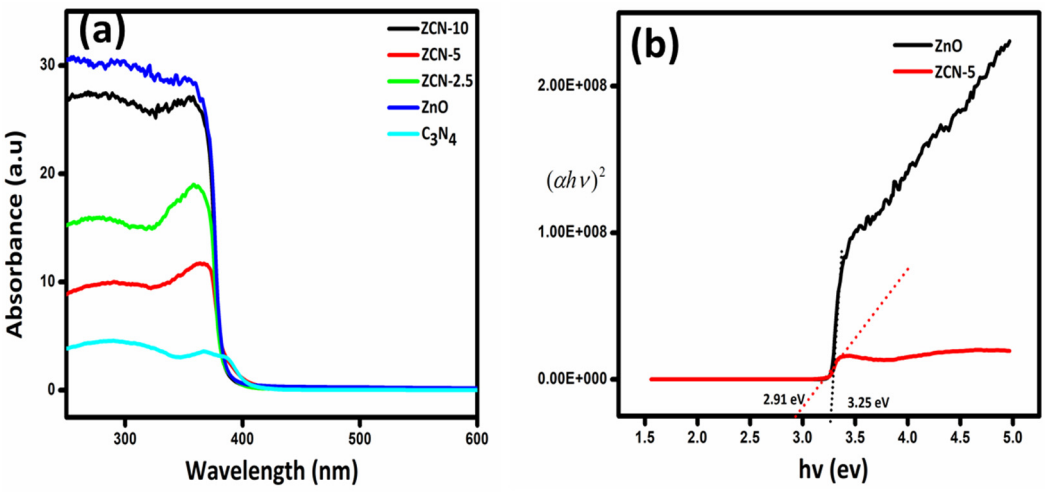


Figure 3. (**a**) UV DRS spectra ZnO and composites of ZnO/C_3N_4; (**b**) Tauc plot of ZnO and composites of ZnO/C_3N_4(ZCN-5).

Figure 4 illustrates the photoluminescence spectra of ZnO/C_3N_4 composites at the excitation wavelength of 325 nm. The ZnO/C_3N_4 composites displayed weak PL emission intensity, compared with C_3N_4, which reduced the recombination of photogenerated charge carriers. There was the lowest PL intensity for ZCN-5 among the other ZnO/C_3N_4 composites, thus showing the efficiency for the separation of the photogenerated electrons and holes [69,70].

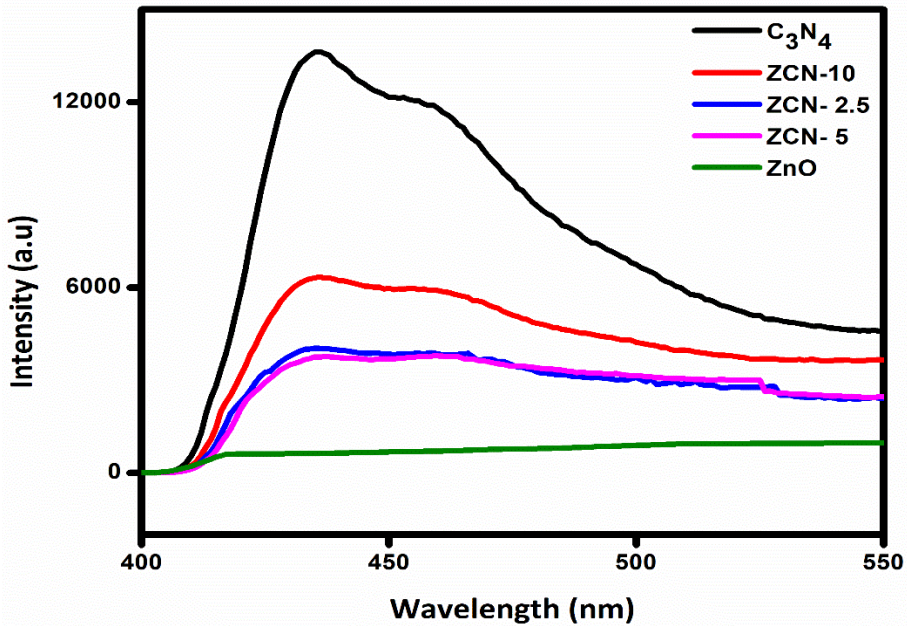


Figure 4. PL spectra of composites of ZnO/C_3N_4.

The morphological and microstructural features of ZnO/C_3N_4 (ZCN-5) were analyzed using transmission electron microscopy (TEM). TEM images of uniformly decorated ZnO on a C_3N_4 sheet under various magnifications are shown in Figure 5a,b. The selected area electron diffraction (SAED) pattern of ZnO/C_3N_4 (ZCN-5) is exhibited in Figure 5c. The composite exhibited a polycrystalline structure, as inferred from the SAED pattern. It

displayed various distinct diffraction rings, which were indexed to the (002) crystal plane of C_3N_4 and the (104) crystal plane of ZnO. The distance of 0.33 nm and 0.278 nm between the adjacent lattice fringes were attributed to the (002) and (104) crystal planes of C_3N_4 and ZnO, as shown in Figure 5d.

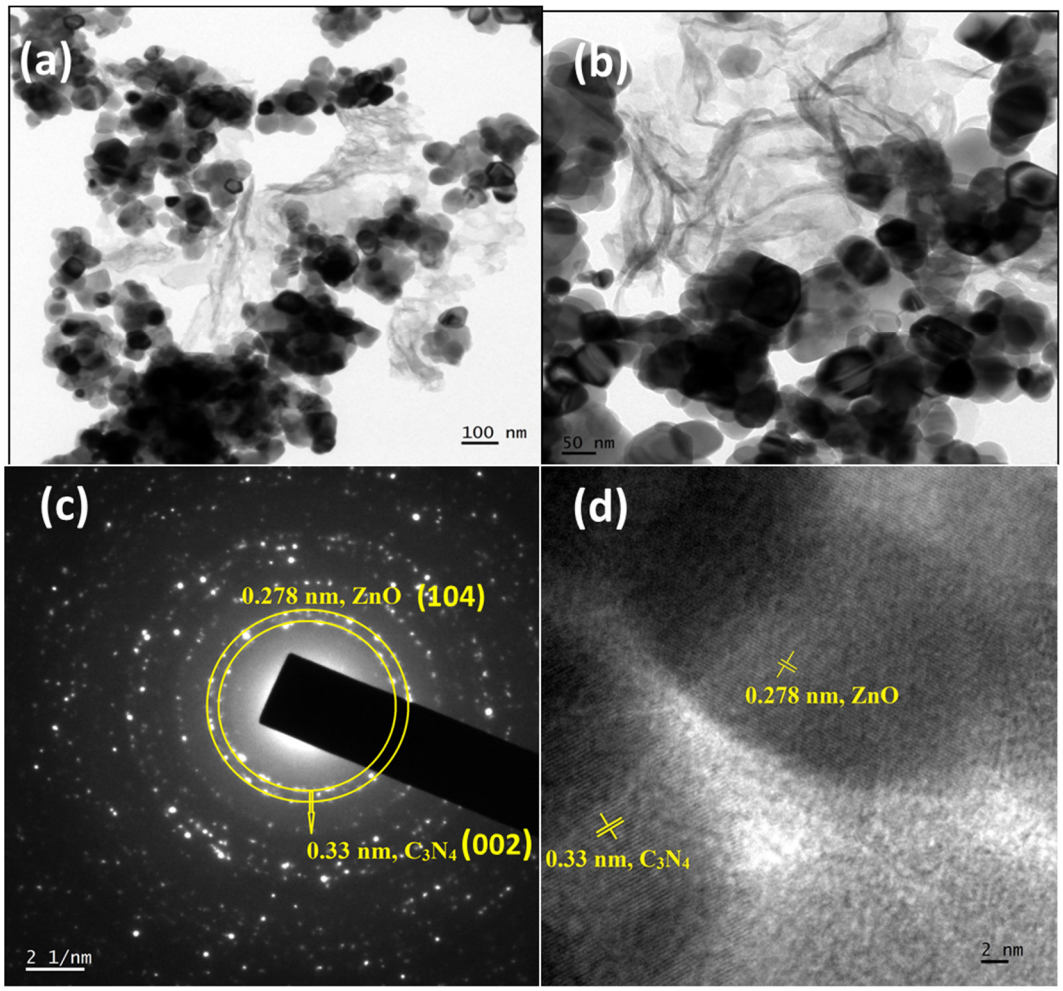


Figure 5. (**a**,**b**) TEM images of ZnO/C_3N_4 (ZCN-5); (**c**) SAED pattern showing the d spacing of different lattice planes in ZnO/C_3N_4 (ZCN-5); (**d**) HRTEM image of ZnO/C_3N_4 (ZCN-5).

The XPS survey spectrum of ZnO/C_3N_4 (ZCN-5) composites showed clear peaks of Zn, O, C, and N. The three characteristic peaks from the high-resolution XPS of C 1s (Figure 6b) were observed at 284.8 eV, 286.5 eV, and 288.8 eV designated to the C-C bonds, graphitic carbon (C=N) in the s-triazine rings, and sp^3-bonded carbon (C-N), respectively. The two characteristic peaks from the high-resolution XPS of N 1s (Figure 6c) were observed at 399.3 eV, and 400.7 eV, ascribed to sp^2 N of the triazine ring and the tertiary nitrogen N–$(C)_3$. The peak at 402.6 eV was ascribed to the amine functions (–NH_x). Figure 6d shows the high-resolution XPS of O 1s, at 532.1 and 532.8 eV, corresponding to the lattice oxygen in the ZnO particles decorated on the C_3N_4 nanosheet. The high-resolution XPS of Zn 2p was split into the Zn $2p_{1/2}$ (1044.7 eV) and $2p_{3/2}$ (1021.6 eV), as shown in Figure 6e [31].

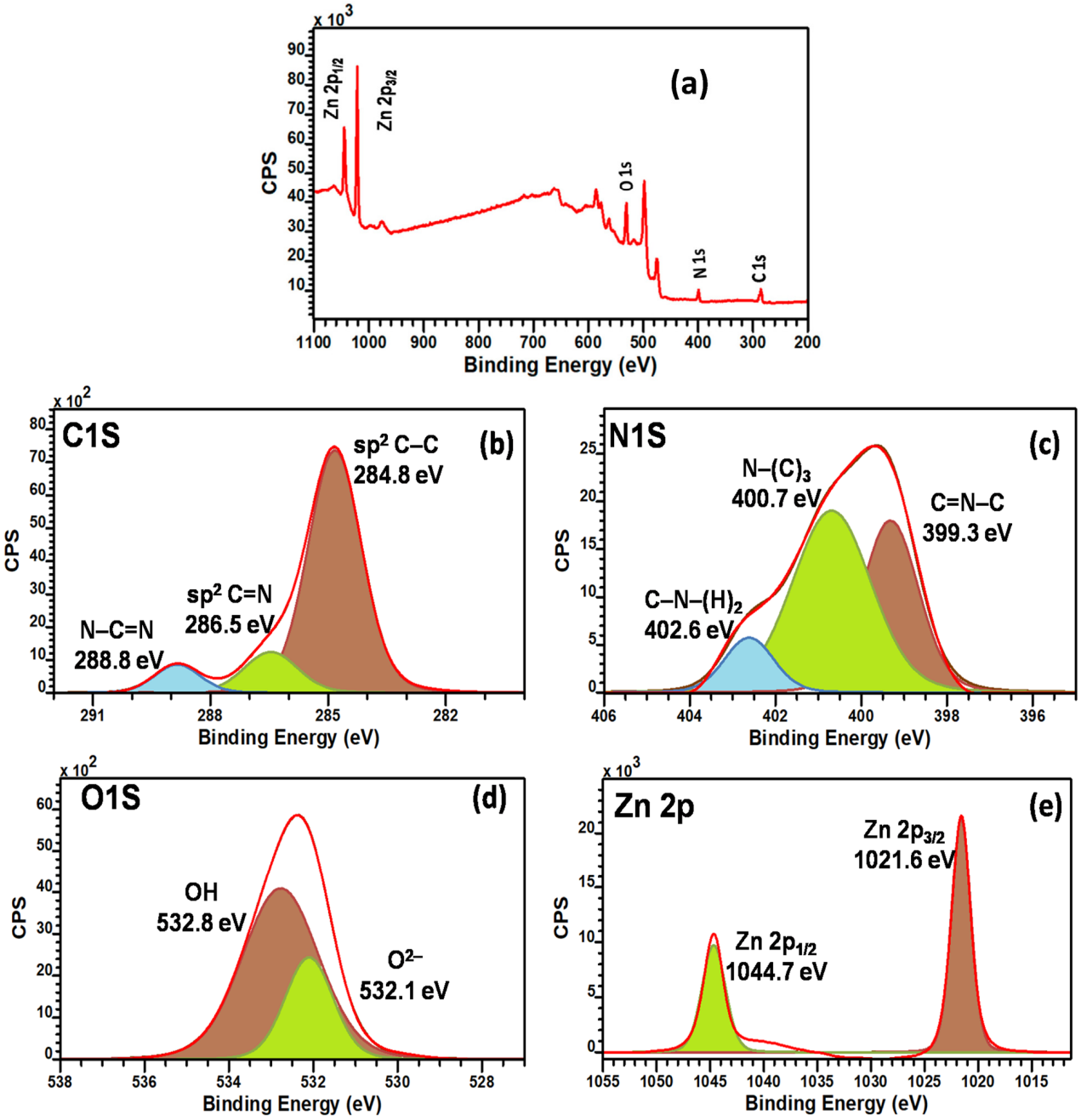


Figure 6. (**a**) Survey spectra, (**b**) C 1s, (**c**) N 1s (**d**) O 1s, and (**e**) Zn 2p XPS spectra of ZCN-5.

The BET-specific surface areas of ZnO and ZnO/C_3N_4 (ZCN-5) were found to be 33 and 61 m^2/g, respectively. A typical type III isotherm with a hysteresis loop was observed in ZnO/C_3N_4 (ZCN-5). The high surface area of the composite provided more active sites. resulting in high photocatalytic activity for the ZCN-5 composite (Figure 7).

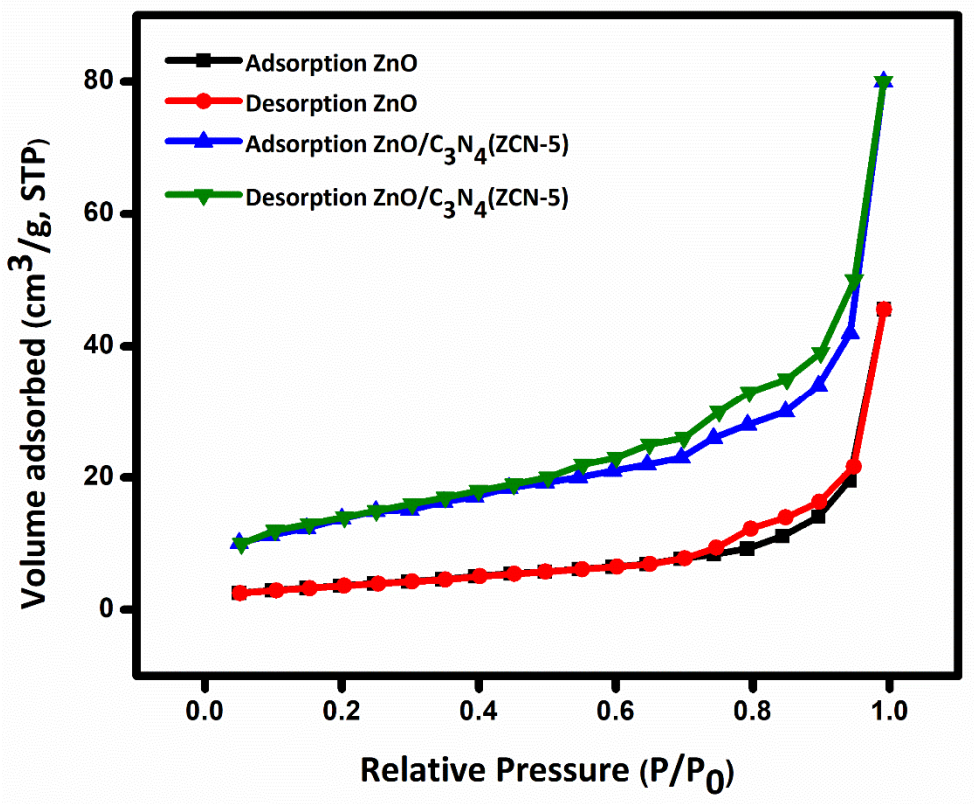


Figure 7. N_2 adsorption–desorption isotherms of ZnO/C_3N_4 (ZCN-5) and ZnO.

4. Degradation of Rhodamine B under Sunlight

The catalytic activities of the ZnO/C_3N_4 composites under sunlight were analyzed by examining the photocatalytic removal of rhodamine B (RhB). In a typical procedure, 60 mg of the photocatalyst was added to 50 mL of a 10 ppm (RhB) solution. Equilibrium was achieved by stirring the reaction mixture for 1 h in the dark. Then, the suspension was kept under sunlight. The solution was placed under sunlight for 70 min (60,000–65,000 lux, 12:00 p.m. to 2:00 p.m., 2 March 2020, Kottayam, Kerala, India; geographical location: 9°39′38.7″ north, 76°32′01.7″ east). The concentration of RhB was examined based on the absorbance at 554 nm using a UV–Vis spectrophotometer.

5. Photocatalytic Activities

The photocatalytic activity of the 0D/2D heterojunction composite, ZnO/C_3N_4 derived from the ZIF-8/C_3N_4 binary composite, was studied through the degradation of rhodamine B (RhB) under sunlight. Changes in the concentration of RhB at specified intervals of time were observed for ZnO/C_3N_4 composites with varying wt% of C_3N_4 (ZCN-2.5, ZCN-5, and ZCN-10), and the degradation curves of RhB are shown Figure 8**.** ZCN-5 was the effective photocatalyst from the degradation reaction of the composites. We found that the degradation efficiencies of ZnO and ZCN-5 were 64% and 95% under sunlight in 70 min, as shown in Figure 8. ZCN-5 revealed higher efficiency (95%) than ZCN-2.5 and ZCN-10, which degraded RhB by 81% and 60% in 70 min. There was a detrimental effect on photocatalytic activity by increasing the amount of C_3N_4 to 10 wt%. This can be explained by the reduced number of active sites of ZnO covering excess C_3N_4.

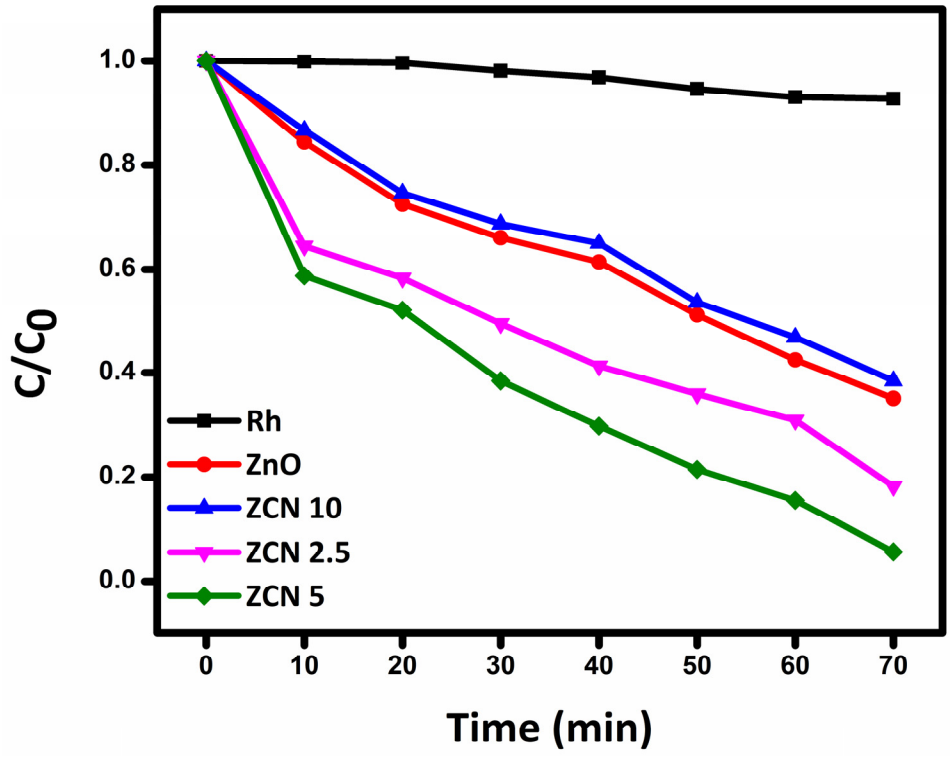


Figure 8. Photocatalytic degradation curves of RhB by ZnO and its composites ZnO/C_3N_4.

A scavenger study was carried out to find the main active species responsible for the degradation process, which helps to realize the photocatalytic mechanism of ZnO/C_3N_4. In this study, the electron, the superoxide radical, and the hole scavengers were silver nitrate ($AgNO_3$), benzoquinone (BQ), and ethylenediaminetetraacetate (EDTA), respectively. As shown in Figure 9, $\bullet O_2^-$ and h^+ radicals were the main species responsible for the degradation process since the degradation of RhB was reduced by adding BQ and EDTA. The addition of $AgNO_3$ induced a small change in the photocatalytic degradation efficiency of RhB. This indicates that electrons had a minor role in the degradation process under sunlight.

Based on the investigation, the schematic diagram of the photocatalytic mechanism of the ZnO/C_3N_4 photocatalyst is displayed in Scheme 2. When ZnO/C_3N_4 (ZCN-5) was irradiated under sunlight, the electrons moved from the valence band (VB) of C_3N_4 to the conduction band (CB), resulting in holes in VB and electrons in CB of C_3N_4. These charged species (electrons and holes) further facilitated the degradation of RhB. The quick recombination of charge carriers could be efficiently inhibited by coupling C_3N_4 with ZnO to form 0D/2D heterojunctions. As a result, the photogenerated electrons from the CB of C_3N_4 transferred to the CB of ZnO and reacted with adsorbed O_2 molecules to generate $\bullet O_2^-$ radicals. This led to improved photogenerated charge carrier separation, hence boosting the process of interfacial electron transfer. Moreover, the photogenerated holes had a strong oxidization capacity for degrading RhB.

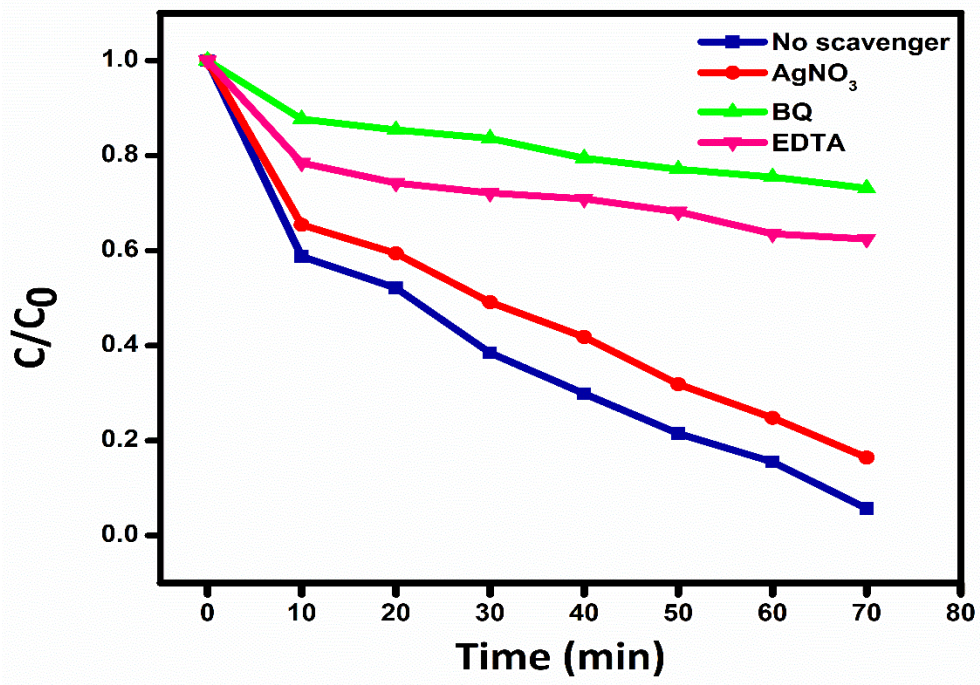
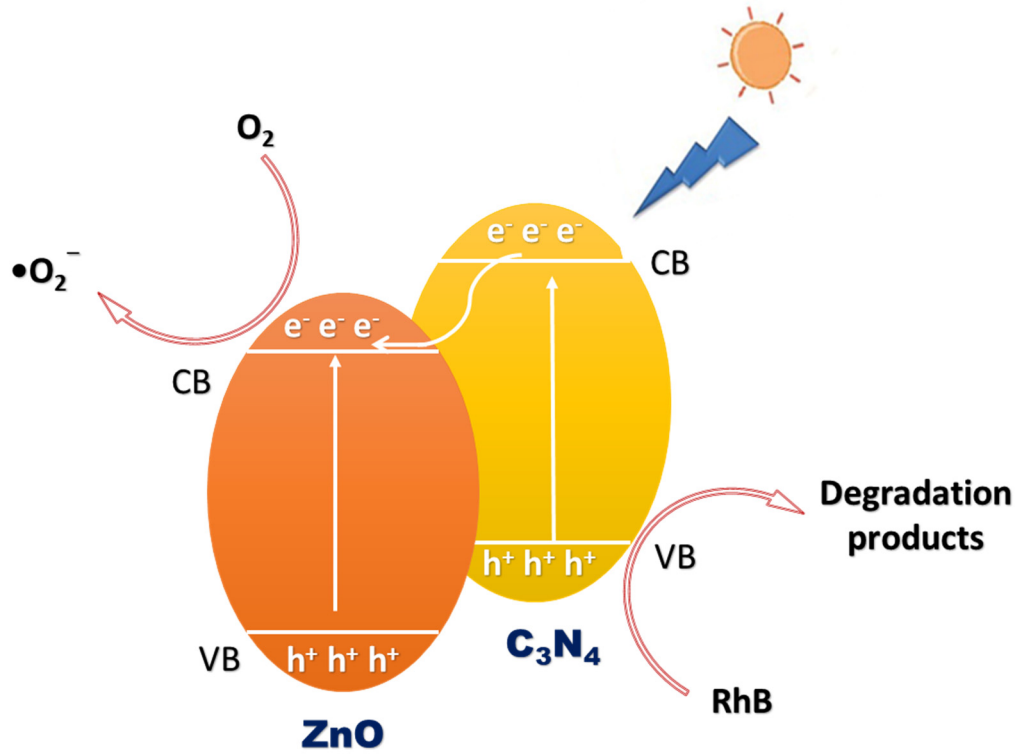


Figure 9. The photodegradation of RhB using different scavengers on ZnO/C_3N_4 under sunlight.



Scheme 2. Schematic design of the photoelectron transfer mechanism in ZnO/C_3N_4.

The stability and reusability of photocatalysts are significant for practical applications. Therefore, the most efficient ZCN-5 was tested for three consecutive cycles for RhB degradation under sunlight (Figure 10). ZCN-5 exhibited excellent stability, as there was no remarkable degradation during three consecutive reactions.

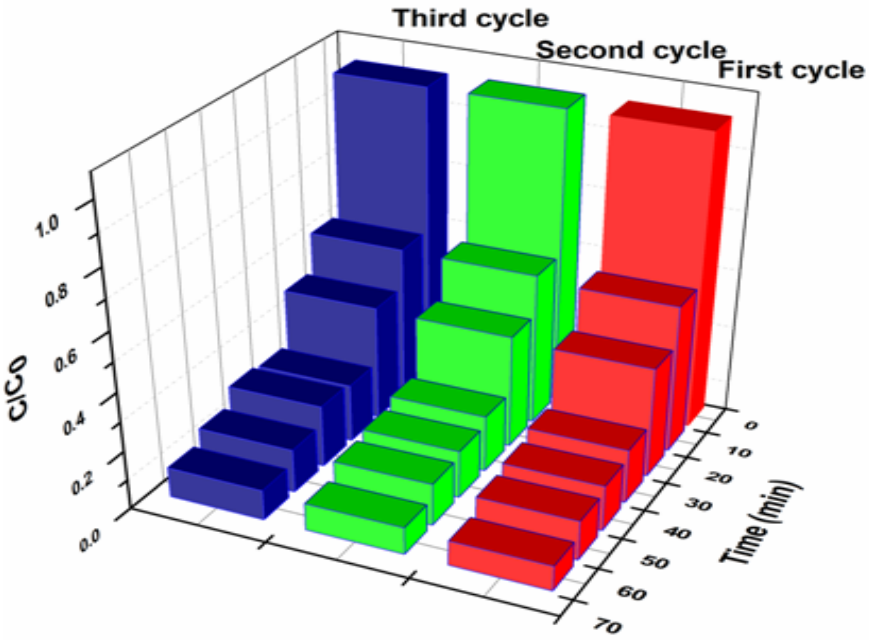


Figure 10. The reusability of ZnO/C_3N_4 for the photodegradation of RhB.

6. Conclusions

The ZnO/C_3N_4 0D/2D heterojunction photocatalysts were prepared via the calcination of ZIF-8/C_3N_4 composites for the photocatalytic process. ZIF-8 acted as a matrix for ZnO, containing a number of active sites that provided close contact with C_3N_4 to favor charge transport between C_3N_4 and ZnO. ZnO-derived ZIF-8 with C_3N_4 (ZCN-5) exhibited excellent catalytic activity, showing 95% degradation of RhB in 70 min, compared with ZnO under sunlight. As a result of the strong interfacial coupling between C_3N_4 and ZnO, the separation of charge carriers was induced, and therefore ZCN-5 showed higher photocatalytic activity.

Supplementary Materials: The following supporting information can be downloaded at: https://www.mdpi.com/article/10.3390/cryst13010047/s1.

Author Contributions: Conceptualization, N.N.A. and S.M.; methodology, N.N.A. and V.P.V.; software, V.T.B.; validation, N.N.A. and S.M.; formal analysis, V.P.V., V.T.B. and B.V.V.; investigation, V.P.V. and N.N.A.; resources, V.T.B.; data curation, N.N.A.; writing—original draft preparation, N.N.A. and S.M.; writing—review and editing, N.N.A. and S.M.; visualization, V.P.V.; supervision, S.M.; project administration, S.M. All authors have read and agreed to the published version of the manuscript.

Funding: This research received no external funding.

Data Availability Statement: Not applicable.

Acknowledgments: We acknowledge Divya K.S., Umadevi T.U., Jisna Jos, Marylin Mary Xavier, Aswathy Joseph, Gladiya Mani, Sreerenjini C.R., Bhagyalakshmi Balan, and Olive Abraham for productive discussions (Mahatma Gandhi University). We thank Soorya Sasi and Sithara Gopinath for their support and help (Research Scholars of Suresh Mathew, Mahatma Gandhi University, Kottayam).

Conflicts of Interest: The authors declare no conflict of interest.

References

1. Tan, H.L.; Abdi, F.F.; Ng, Y.H. Heterogeneous photocatalysts: An overview of classic and modern approaches for optical, electronic, and charge dynamics evaluation. *Chem. Soc. Rev.* **2019**, *48*, 1255–1271. [CrossRef] [PubMed]
2. Reddy, C.V.; Reddy, K.R.; Shetti, N.P.; Shim, J.; Aminabhavi, T.M.; Dionysiou, D.D. Hetero-nanostructured metal oxide-based hybrid photocatalysts for enhanced photoelectrochemical water splitting—A review. *Int. J. Hydrogen Energy* **2020**, *45*, 18331–18347. [CrossRef]

3. Ong, C.B.; Ng, L.Y.; Mohammad, A.W. A review of ZnO nanoparticles as solar photocatalysts: Synthesis, mechanisms and applications. *Renew. Sustain. Energy Rev.* **2018**, *81*, 536–551. [CrossRef]
4. Biasotto, G.; Ranieri, M.; Foschini, C.; Simões, A.; Longo, E.; Zaghete, M. Gas sensor applications of zinc oxide thin film grown by the polymeric precursor method. *Ceram. Int.* **2014**, *40*, 14991–14996. [CrossRef]
5. Deschanvres, J.; Rey, P.; Delabouglise, G.; Labeau, M.; Joubert, J.; Peuzin, J. Characterization of piezoelectric properties of zinc oxide thin films deposited on silicon for sensors applications. *Sens. Actuators A Phys.* **1992**, *33*, 43–45. [CrossRef]
6. Huang, J.; Yin, Z.; Zheng, Q. Applications of ZnO in organic and hybrid solar cells. *Energy Environ. Sci.* **2011**, *4*, 3861–3877. [CrossRef]
7. Tiwari, V.; Mishra, N.; Gadani, K.; Solanki, P.; Shah, N.A.; Tiwari, M. Mechanism of Anti-bacterial Activity of Zinc Oxide Nanoparticle Against Carbapenem-Resistant Acinetobacter baumannii. *Front. Microbiol.* **2018**, *9*, 1218. [CrossRef]
8. Djurišić, A.B.; Chen, X.; Leung, Y.H.; Ng, A.M.C. ZnO nanostructures: Growth, properties and applications. *J. Mater. Chem.* **2012**, *22*, 6526–6535. [CrossRef]
9. Boruah, B.D. Zinc oxide ultraviolet photodetectors: Rapid progress from conventional to self-powered photodetectors. *Nanoscale Adv.* **2019**, *1*, 2059–2085. [CrossRef]
10. Rajamanickam, D.; Shanthi, M. Photocatalytic degradation of an organic pollutant by zinc oxide—solar process. *Arab. J. Chem.* **2016**, *9*, S1858–S1868. [CrossRef]
11. Rauf, M.; Ashraf, S.S. Fundamental principles and application of heterogeneous photocatalytic degradation of dyes in solution. *Chem. Eng. J.* **2009**, *151*, 10–18. [CrossRef]
12. Sun, J.-H.; Dong, S.-Y.; Wang, Y.-K.; Sun, S.-P. Preparation and photocatalytic property of a novel dumbbell-shaped ZnO microcrystal photocatalyst. *J. Hazard. Mater.* **2009**, *172*, 1520–1526. [CrossRef]
13. Klingshirn, C. ZnO: Material, Physics and Applications. *ChemPhysChem* **2007**, *8*, 782–803. [CrossRef]
14. Zhang, J.-Y.; Mei, J.-Y.; Yi, S.-S.; Guan, X.-X. Constructing of Z-scheme 3D g-C_3N_4-ZnO@graphene aerogel heterojunctions for high-efficient adsorption and photodegradation of organic pollutants. *Appl. Surf. Sci.* **2019**, *492*, 808–817. [CrossRef]
15. Wang, S.; Zhu, B.; Liu, M.; Zhang, L.; Yu, J.; Zhou, M. Direct Z-scheme ZnO/CdS hierarchical photocatalyst for enhanced photocatalytic H_2-production activity. *Appl. Catal. B* **2019**, *243*, 19–26. [CrossRef]
16. Qi, K.; Xing, X.; Zada, A.; Li, M.; Wang, Q.; Liu, S.-Y.; Lin, H.; Wang, G. Transition metal doped ZnO nanoparticles with enhanced photocatalytic and antibacterial performances: Experimental and DFT studies. *Ceram. Int.* **2019**, *46*, 1494–1502. [CrossRef]
17. Kabir, R.; Saifullah, A.K.; Ahmed, A.Z.; Masum, S.; Molla, A.I. Synthesis of N-Doped ZnO Nanocomposites for Sunlight Photocatalytic Degradation of Textile Dye Pollutants. *J. Compos. Sci.* **2020**, *4*, 49. [CrossRef]
18. Prabakaran, E.; Pillay, K. Synthesis of N-doped ZnO nanoparticles with cabbage morphology as a catalyst for the efficient photocatalytic degradation of methylene blue under UV and visible light. *RSC Adv.* **2019**, *9*, 7509–7535. [CrossRef]
19. Raizada, P.; Sudhaik, A.; Singh, P. Photocatalytic water decontamination using graphene and ZnO coupled photocatalysts: A review. *Mater. Sci. Energy Technol.* **2019**, *2*, 509–525. [CrossRef]
20. Barrio, J.; Volokh, M.; Shalom, M. Polymeric carbon nitrides and related metal-free materials for energy and environmental applications. *J. Mater. Chem. A* **2020**, *8*, 11075–11116. [CrossRef]
21. Zhou, Z.; Zhang, Y.; Shen, Y.; Liu, S.; Zhang, Y. Molecular engineering of polymeric carbon nitride: Advancing applications from photocatalysis to biosensing and more. *Chem. Soc. Rev.* **2018**, *47*, 2298–2321. [CrossRef]
22. Wang, Y.; Wang, X.; Antonietti, M. Polymeric Graphitic Carbon Nitride as a Heterogeneous Organocatalyst: From Photochemistry to Multipurpose Catalysis to Sustainable Chemistry. *Angew. Chem. Int. Ed.* **2012**, *51*, 68–89. [CrossRef]
23. Ismael, M.; Wu, Y. A mini-review on the synthesis and structural modification of g-C_3N_4-based materials, and their applications in solar energy conversion and environmental remediation. *Sustain. Energy Fuels* **2019**, *3*, 2907–2925. [CrossRef]
24. Rono, N.; Kibet, J.K.; Martincigh, B.S.; Nyamori, V.O. A review of the current status of graphitic carbon nitride. *Crit. Rev. Solid State Mater. Sci.* **2020**, *46*, 189–217. [CrossRef]
25. Zhang, H.-G.; Feng, L.-J.; Li, C.-H.; Wang, L. Preparation of graphitic carbon nitride with nitrogen-defects and its photocatalytic performance in the degradation of organic pollutants under visible light. *J. Fuel Chem. Technol.* **2018**, *46*, 871–878. [CrossRef]
26. Xavier, M.M.; Nair, P.R.; Mathew, S. Emerging trends in sensors based on carbon nitride materials. *Analyst* **2019**, *144*, 1475–1491. [CrossRef] [PubMed]
27. Liu, B.; Xu, B.; Li, S.; Du, J.; Liu, Z.; Zhong, W. Heptazine-based porous graphitic carbon nitride: A visible-light driven photocatalyst for water splitting. *J. Mater. Chem. A* **2019**, *7*, 20799–20805. [CrossRef]
28. Ehrmaier, J.; Karsili, T.N.V.; Sobolewski, A.L.; Domcke, W. Mechanism of Photocatalytic Water Splitting with Graphitic Carbon Nitride: Photochemistry of the Heptazine–Water Complex. *J. Phys. Chem. A* **2017**, *121*, 4754–4764. [CrossRef] [PubMed]
29. Volokh, M.; Peng, G.; Barrio, J.; Shalom, M. Carbon Nitride Materials for Water Splitting Photoelectrochemical Cells. *Angew. Chem. Int. Ed.* **2019**, *58*, 6138–6151. [CrossRef]
30. Chetia, T.R.; Ansari, M.S.; Qureshi, M. Graphitic carbon nitride as a photovoltaic booster in quantum dot sensitized solar cells: A synergistic approach for enhanced charge separation and injection. *J. Mater. Chem. A* **2016**, *4*, 5528–5541. [CrossRef]
31. Paul, D.R.; Gautam, S.; Panchal, P.; Nehra, S.P.; Choudhary, P.; Sharma, A. ZnO-Modified g-C_3N_4: A Potential Photocatalyst for Environmental Application. *ACS Omega* **2020**, *5*, 3828–3838. [CrossRef] [PubMed]

32. Yuan, X.; Duan, S.; Wu, G.; Sun, L.; Cao, G.; Li, D.; Xu, H.; Li, Q.; Xia, D. Enhanced catalytic ozonation performance of highly stabilized mesoporous ZnO doped g-C 3 N 4 composite for efficient water decontamination. *Appl. Catal. A* **2018**, *551*, 129–138. [CrossRef]
33. Le, S.; Jiang, T.; Li, Y.; Zhao, Q.; Li, Y.; Fang, W.; Gong, M. Highly efficient visible-light-driven mesoporous graphitic carbon nitride/ZnO nanocomposite photocatalysts. *Appl. Catal. B* **2017**, *200*, 601–610. [CrossRef]
34. Liu, Y.; Liu, H.; Zhou, H.; Li, T.; Zhang, L. A Z-scheme mechanism of N-ZnO/g-C_3N_4 for enhanced H_2 evolution and photocatalytic degradation. *Appl. Surf. Sci.* **2019**, *466*, 133–140. [CrossRef]
35. Kočí, K.; Reli, M.; Troppová, I.; Šihor, M.; Bajcarová, T.; Ritz, M.; Pavlovský, J.; Praus, P. Photocatalytic Decomposition of N_2O by Using Nanostructured Graphitic Carbon Nitride/Zinc Oxide Photocatalysts Immobilized on Foam. *Catalysts* **2019**, *9*, 735. [CrossRef]
36. Gao, X.; Yang, B.; Yao, W.; Wang, Y.; Zong, R.; Wang, J.; Li, X.; Jin, W.; Tao, D. Enhanced photocatalytic activity of ZnO/g-C_3N_4 composites by regulating stacked thickness of g-C_3N_4 nanosheets. *Environ. Pollut.* **2020**, *257*, 113577. [CrossRef]
37. Yang, H.; Jin, Z.; Hu, H.; Lu, G.; Bi, Y. Fivefold Enhanced Photoelectrochemical Properties of ZnO Nanowire Arrays Modified with C_3N_4 Quantum Dots. *Catalysts* **2017**, *7*, 99. [CrossRef]
38. Guan, R.; Li, J.; Zhang, J.; Zhao, Z.; Wang, D.; Zhai, H.; Sun, D. Photocatalytic Performance and Mechanistic Research of ZnO/g-C_3N_4 on Degradation of Methyl Orange. *ACS Omega* **2019**, *4*, 20742–20747. [CrossRef]
39. Moussa, H.; Chouchene, B.; Gries, T.; Balan, L.; Mozet, K.; Medjahdi, G.; Schneider, R. Growth of ZnO Nanorods on Graphitic Carbon Nitride gCN Sheets for the Preparation of Photocatalysts with High Visible-Light Activity. *ChemCatChem* **2018**, *10*, 4987–4997. [CrossRef]
40. Sett, A.; Das, D.; Banerjee, D.; Ghorai, U.K.; Das, N.S.; Das, B.; Chattopadhyay, K.K. 1D–2D hybrids as efficient optoelectronic materials: A study on graphitic carbon nitride nanosheets wrapped with zinc oxide rods. *Dalton Trans.* **2018**, *47*, 4501–4507. [CrossRef]
41. Zhang, Y.; Yan, M.; Ge, S.; Ma, C.; Yu, J.; Song, X. An enhanced photoelectrochemical platform: Graphite-like carbon nitride nanosheet-functionalized ZnO nanotubes. *J. Mater. Chem. B* **2016**, *4*, 4980–4987. [CrossRef] [PubMed]
42. Fageria, P.; Nazir, R.; Gangopadhyay, S.; Barshilia, H.C.; Pande, S. Graphitic-carbon nitride support for the synthesis of shape-dependent ZnO and their application in visible light photocatalysts. *RSC Adv.* **2015**, *5*, 80397–80409. [CrossRef]
43. Qin, H.; Zuo, Y.; Jin, J.; Wang, W.; Xu, Y.; Cui, L.; Dang, H. ZnO nanorod arrays grown on g-C_3N_4 micro-sheets for enhanced visible light photocatalytic H_2 evolution. *RSC Adv.* **2019**, *9*, 24483–24488. [CrossRef] [PubMed]
44. Mahala, C.; Sharma, M.D.; Basu, M. ZnO Nanosheets Decorated with Graphite-Like Carbon Nitride Quantum Dots as Photoanodes in Photoelectrochemical Water Splitting. *ACS Appl. Nano Mater.* **2020**, *3*, 1999–2007. [CrossRef]
45. Kumar, S.; Kumar, A.; Kumar, A.; Balaji, R.; Krishnan, V. Highly Efficient Visible Light Active 2D-2D Nanocomposites of N-ZnO-g-C_3 N_4 for Photocatalytic Degradation of Diverse Industrial Pollutants. *Chemistryselect* **2018**, *3*, 1919–1932. [CrossRef]
46. Kalisamy, P.; Lallimathi, M.; Suryamathi, M.; Palanivel, B.; Venkatachalam, M. ZnO-embedded S-doped g-C_3N_4 heterojunction: Mediator-free Z-scheme mechanism for enhanced charge separation and photocatalytic degradation. *RSC Adv.* **2020**, *10*, 28365–28375. [CrossRef]
47. Rasheed, H.U.; Lv, X.; Wei, W.; Yaseen, W.; Ullah, N.; Xie, J.; Zhu, W. Synthesis and studies of ZnO doped with g-C_3N_4 nanocomposites for the degradation of tetracycline hydrochloride under the visible light irradiation. *J. Environ. Chem. Eng.* **2019**, *7*, 103152. [CrossRef]
48. Li, Z.; Mei, J.; Bai, L. Synthesis of C_3N_4-decorated ZnO and Ag/ZnO nanoparticles via calcination of ZIF-8 and melamine for photocatalytic removal of methyl orange. *Chem. Pap.* **2019**, *73*, 883–889. [CrossRef]
49. Li, N.; Tian, Y.; Zhao, J.; Zhang, J.; Zuo, W.; Kong, L.; Cui, H. Z-scheme 2D/3D g-C_3N_4@ZnO with enhanced photocatalytic activity for cephalexin oxidation under solar light. *Chem. Eng. J.* **2018**, *352*, 412–422. [CrossRef]
50. Xavier, M.M.; George, J.; Divya, K.S.; Adarsh, N.N.; Nair, P.R.; Mathew, S. Green Synthesis of a Metal-Free 0D/2D Heterojunction: A Cost-Effective Approach. *ChemistrySelect* **2019**, *4*, 11541–11547. [CrossRef]
51. Yaghi, O.M.; O'Keeffe, M.; Ockwig, N.W.; Chae, H.K.; Eddaoudi, M.; Kim, J. Reticular synthesis and the design of new materials. *Nature* **2003**, *423*, 705–714. [CrossRef] [PubMed]
52. Furukawa, H.; Cordova, K.E.; O'Keeffe, M.; Yaghi, O.M. The Chemistry and Applications of Metal-Organic Frameworks. *Science* **2013**, *341*, 1230444. [CrossRef] [PubMed]
53. Schneemann, A.; Bon, V.; Schwedler, I.; Senkovska, I.; Kaskel, S.; Fischer, R.A. Flexible metal–organic frameworks. *Chem. Soc. Rev.* **2014**, *43*, 6062–6096. [CrossRef]
54. Kitagawa, S.; Kitaura, R.; Noro, S.-I. Functional Porous Coordination Polymers. *Angew. Chem. Int. Ed.* **2004**, *43*, 2334–2375. [CrossRef]
55. Janiak, C. Engineering coordination polymers towards applications. *Dalton Trans.* **2003**, *14*, 2781–2804. [CrossRef]
56. Adarsh, N.N.; Dastidar, P. Coordination polymers: What has been achieved in going from innocent 4,4′-bipyridine to bis-pyridyl ligands having a non-innocent backbone? *Chem. Soc. Rev.* **2012**, *41*, 3039–3060. [CrossRef] [PubMed]
57. Adarsh, N.N. *Metal-Organic Framework (MOF)—Derived Metal Oxides for Supercapacitors*, 7th Chapter; Dubal, D.P., Romero, P.G., Eds.; Metal Oxides in Supercapacitors; Elsevier: Amsterdam, The Netherlands, 2017; pp. 165–192. [CrossRef]
58. Salunkhe, R.R.; Kaneti, Y.V.; Yamauchi, Y. Metal–Organic Framework-Derived Nanoporous Metal Oxides toward Supercapacitor Applications: Progress and Prospects. *ACS Nano* **2017**, *11*, 5293–5308. [CrossRef] [PubMed]

59. An, C.; Zhang, Y.; Guo, H.; Wang, Y. Metal oxide-based supercapacitors: Progress and prospectives. *Nanoscale Adv.* **2019**, *1*, 4644–4658. [CrossRef]
60. Zou, G.; Hou, H.; Ge, P.; Huang, Z.; Zhao, G.; Yin, D.; Ji, X. Metal-Organic Framework-Derived Materials for Sodium Energy Storage. *Small* **2018**, *14*, 1702648. [CrossRef]
61. Chen, T.; Liu, X.; Niu, L.; Gong, Y.; Li, C.; Xu, S.; Pan, L. Recent progress on metal–organic framework-derived materials for sodium-ion battery anodes. *Inorg. Chem. Front.* **2019**, *7*, 567–582. [CrossRef]
62. Zhao, R.; Liang, Z.; Zou, R.; Xu, Q. Metal-Organic Frameworks for Batteries. *Joule* **2018**, *2*, 2235–2259. [CrossRef]
63. Zhan, W.; Sun, L.; Han, X. Recent Progress on Engineering Highly Efficient Porous Semiconductor Photocatalysts Derived from Metal–Organic Frameworks. *Nano-Micro Lett.* **2019**, *11*, 1. [CrossRef]
64. Oar-Arteta, L.; Wezendonk, T.; Sun, X.; Kapteijn, F.; Gascon, J. Metal organic frameworks as precursors for the manufacture of advanced catalytic materials. *Mater. Chem. Front.* **2017**, *1*, 1709–1745. [CrossRef]
65. Wang, Z.; Li, M.; Ye, Y.; Yang, Y.; Lu, Y.; Ma, X.; Zhang, Z.; Xiang, S. MOF-derived binary mixed carbon/metal oxide porous materials for constructing simultaneous determination of hydroquinone and catechol sensor. *J. Solid State Electrochem.* **2019**, *23*, 81–89. [CrossRef]
66. Xiao, X.; Peng, S.; Wang, C.; Cheng, D.; Li, N.; Dong, Y.; Li, Q.; Wei, D.; Liu, P.; Xie, Z.; et al. Metal/metal oxide@carbon composites derived from bimetallic Cu/Ni-based MOF and their electrocatalytic performance for glucose sensing. *J. Electroanal. Chem.* **2019**, *841*, 94–100. [CrossRef]
67. Qu, F.; Jiang, H.; Yang, M. MOF-derived Co_3O_4/$NiCo_2O_4$ double-shelled nanocages with excellent gas sensing properties. *Mater. Lett.* **2017**, *190*, 75–78. [CrossRef]
68. Mounfield, W.P.; Tumuluri, U.; Jiao, Y.; Li, M.; Dai, S.; Wu, Z.; Walton, K.S. Role of defects and metal coordination on adsorption of acid gases in MOFs and metal oxides: An in situ IR spectroscopic study. *Microporous Mesoporous Mater.* **2016**, *227*, 65–75. [CrossRef]
69. Yap, M.H.; Fow, K.L.; Chen, G.Z. Synthesis and applications of MOF-derived porous nanostructures. *Green Energy Environ.* **2017**, *2*, 218–245. [CrossRef]
70. Banerjee, R.; Phan, A.; Wang, B.; Knobler, C.; Furukawa, H.; O'Keeffe, M.; Yaghi, O.M. High-Throughput Synthesis of Zeolitic Imidazolate Frameworks and Application to CO_2 Capture. *Science* **2008**, *319*, 939–943. [CrossRef]
71. Huang, X.-C.; Lin, Y.-Y.; Zhang, J.-P.; Chen, X.-M. Ligand-Directed Strategy for Zeolite-Type Metal–Organic Frameworks: Zinc(II) Imidazolates with Unusual Zeolitic Topologies. *Angew. Chem. Int. Ed.* **2006**, *45*, 1557–1559. [CrossRef]
72. Fan, J.; Chen, J.; Zhang, Q.; Chen, B.; Zang, J.; Zheng, M.; Dong, Q. An Amorphous Carbon Nitride Composite Derived from ZIF-8 as Anode Material for Sodium-Ion Batteries. *ChemSusChem* **2015**, *8*, 1856–1861. [CrossRef]
73. Kaye, S.S.; Dailly, A.; Yaghi, A.O.M.; Long, J.R. Impact of Preparation and Handling on the Hydrogen Storage Properties of Zn_4O(1,4-benzenedicarboxylate)$_3$ (MOF-5). *J. Am. Chem. Soc.* **2007**, *129*, 14176–14177. [CrossRef] [PubMed]
74. Aleksandrzak, M.; Sielicki, K.; Mijowska, E. Enhancement of photocatalytic hydrogen evolution with catalysts based on carbonized MOF-5 and g-C_3N. *RSC Adv.* **2020**, *10*, 4032–4039. [CrossRef] [PubMed]
75. Liu, W.; Wang, M.; Xu, C.; Chen, S. Facile synthesis of g-C_3N_4/ZnO composite with enhanced visible light photooxidation and photoreduction properties. *Chem. Eng. J.* **2012**, *209*, 386–393. [CrossRef]
76. Nie, N.; Zhang, L.; Fu, J.; Cheng, B.; Yu, J. Self-assembled hierarchical direct Z-scheme g-C_3N_4/ZnO microspheres with enhanced photocatalytic CO_2 reduction performance. *Appl. Surf. Sci.* **2018**, *441*, 12–22. [CrossRef]
77. Yang, X.; Qiu, L.; Luo, X. ZIF-8 derived Ag-doped ZnO photocatalyst with enhanced photocatalytic activity. *RSC Adv.* **2018**, *8*, 4890–4894. [CrossRef]
78. Park, T.J.; Pawar, R.C.; Kang, S.; Lee, C.S. Ultra-thin coating of g-C_3N_4 on an aligned ZnO nanorod film for rapid charge separation and improved photodegradation performance. *RSC Adv.* **2016**, *6*, 89944–89952. [CrossRef]

Disclaimer/Publisher's Note: The statements, opinions and data contained in all publications are solely those of the individual author(s) and contributor(s) and not of MDPI and/or the editor(s). MDPI and/or the editor(s) disclaim responsibility for any injury to people or property resulting from any ideas, methods, instructions or products referred to in the content.